

# DRIFT MODE CALCULATIONS IN NONAXISYMMETRIC GEOMETRY

G. Rewoldt, L.-P. Ku, W.M. Tang

*Princeton Plasma Physics Laboratory*

W.A. Cooper

*CRPP-EPFL*

NCSX Physics Meeting

October 7, 1999



# Code Properties

---

- Start with existing tokamak microinstability code, FULL (*i.e.*, same dynamics)
  - high- $n$  calculation, lowest-order ballooning representation
  - includes trapped particles, FLR effects to all orders, banana orbital dynamics, bounce and transit and magnetic drift frequency resonances, equilibrium shaping effects, etc., for all species
  - Refs: G. Rewoldt, W.M. Tang, and M.S. Chance, Phys. Fluids **25**, 480 (1982); G. Rewoldt, W.M. Tang, and R.J. Hastie, Phys. Fluids **30**, 807 (1987)

- tokamak version uses (axisymmetric) PEST-I flux coordinates, for instance for MHD equilibria calculated by JSOLVER code
- For nonaxisymmetric version, new interface to 3D VMEC MHD equilibrium code (S. Hirshman), in VMEC coordinates
- 3D MHD equilibrium transformed to Boozer coordinates by TERPSICHORE code (W.A. Cooper, *et al.*)
- Data along single chosen magnetic field line constructed by ideal MHD ballooning mode code VVBAL (W.A. Cooper). Data along field line now needed over many periods, not just one period as in axisymmetric case

- Particle turning points along field line found numerically, so all classes of trapped particles included automatically (*i.e.*, both toroidally-trapped and helically-trapped)
- Model Krook collision operator now generalized in way that is usable when there are multiple classes of trapped particles, *i.e.*, one toroidally trapped class and multiple helically-trapped classes
- Changes now implemented in electrostatic version of FULL code
- Nonaxisymmetric code and these results written up in Report PPPL-3354, available on PPPL web pages in PDF and postscript formats

# TOKAMAK TEST CASE

---

- Employ axisymmetric ARIES case, with low  $\beta$  ( $\beta_N = 0.1$ ), taking  $\eta_i = \eta_e = 3.0$ ,  $T_i = T_e = 15.74$  keV, and  $B_0 = 69.17$  kG on chosen magnetic surface (surface 36 of 48), with ballooning parameter  $\theta_0 = 0$
- Use matched MHD equilibria: 2D JSOLVER equilibrium (due to C. Kessel) and 3D VMEC equilibrium with zero helical components
- Results for collisionless electrostatic toroidal drift mode (trapped-electron-ITG mode) with varying  $k_\perp \rho_i(\theta = 0)$  (or equivalently varying toroidal mode number  $n$ ) show good agreement for linear growth rate  $\gamma$  in Fig. 1 and for real frequency  $\omega_r$  in Fig. 2

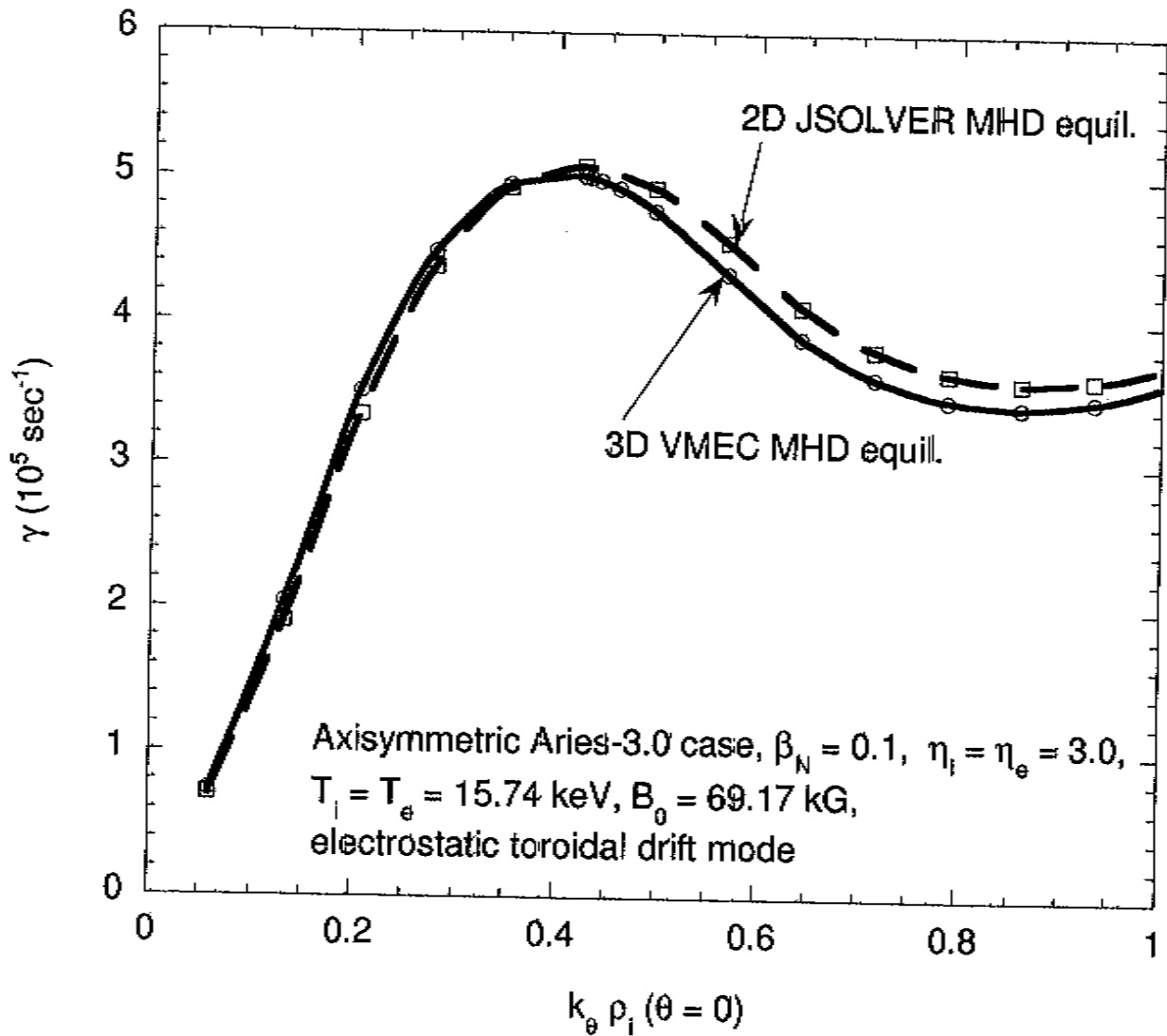


Fig. 1

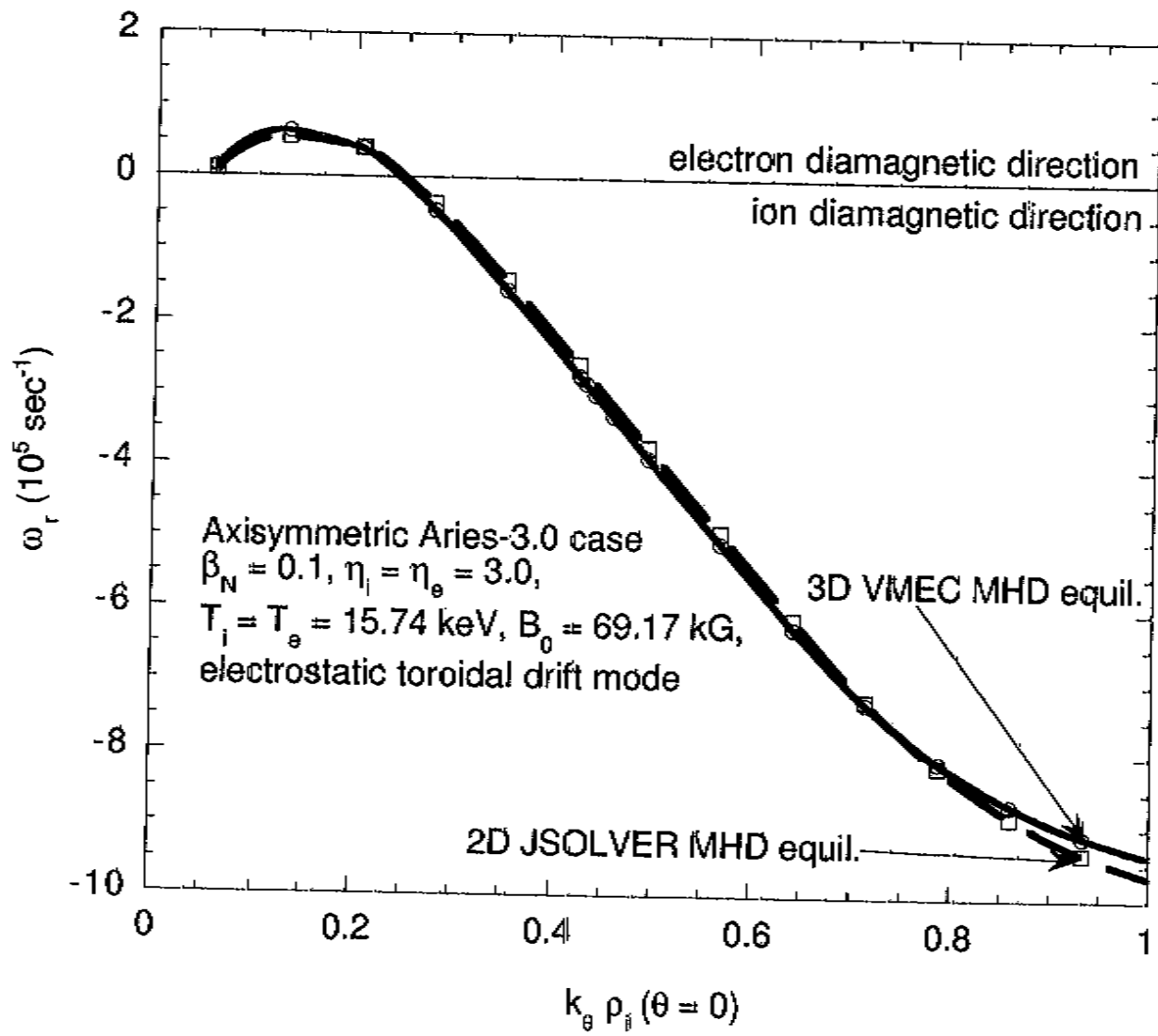


Fig. 2

## C-82 STELLARATOR CASE

---

- Use equilibrium QAS3\_C82 (fixed boundary, very low  $\beta$ ,  $\langle \beta \rangle = 0.01\%$ ), for the NCSX stellarator design
- Input functions on chosen field line on chosen magnetic surface (surface 38 of outer 50,  $s = 0.875$ ), with ballooning parameter  $\theta_0 = 0$  and field line label  $\alpha \equiv \zeta - q\theta = \pi/3 = 1.0472$  shown in Fig. 3 for  $|B(\theta)|$ , in Fig. 4 for  $k_\perp^2(\theta)$ , and in Fig. 5 for the curvature drift  $\equiv \mathbf{k}_\perp \cdot \{\mathbf{b} \times [(\mathbf{b} \cdot \nabla) \mathbf{b}]\}$
- FULL code finds all particle turning points numerically for multiple classes of trapped particles, as illustrated in Fig. 3

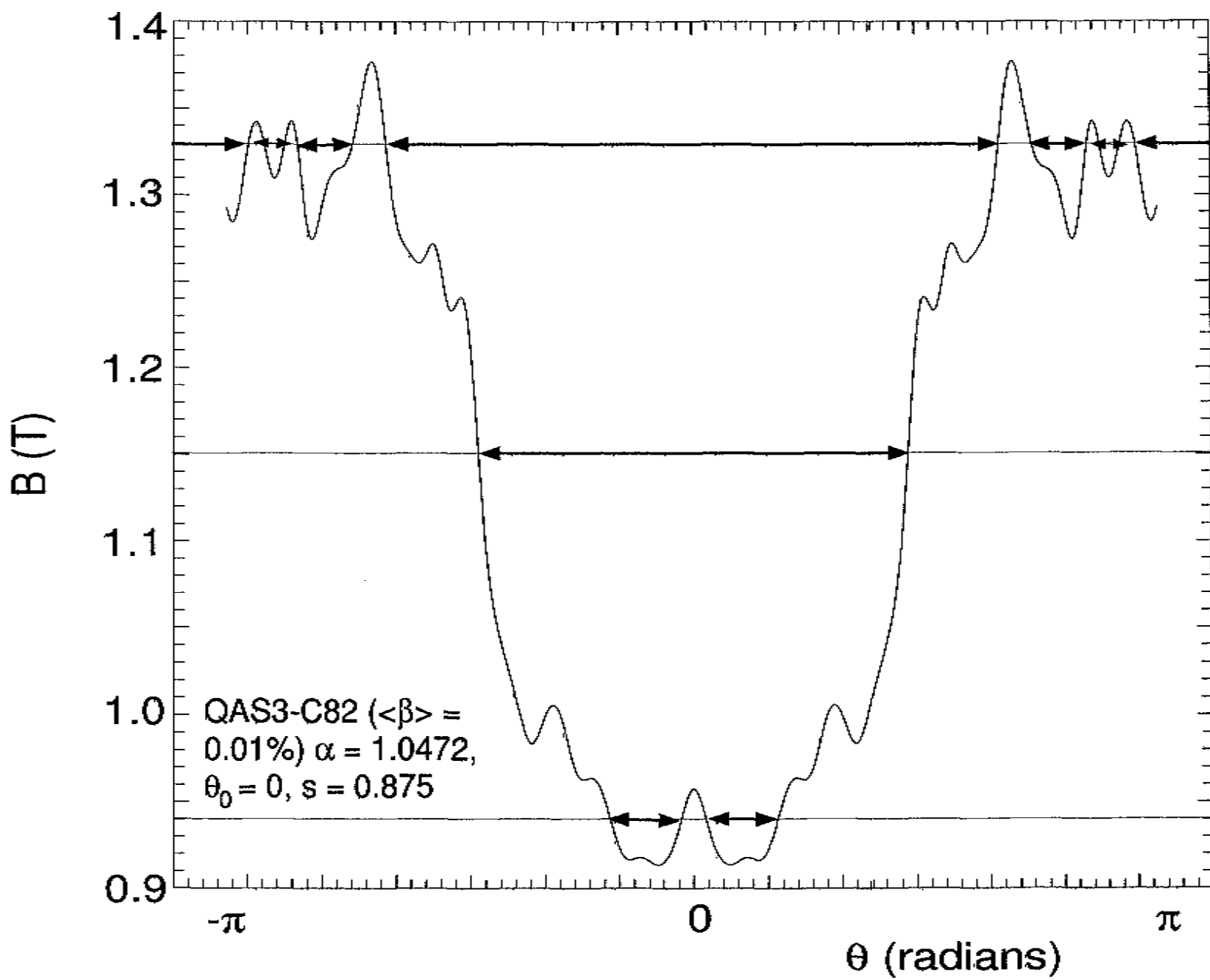


Fig. 3

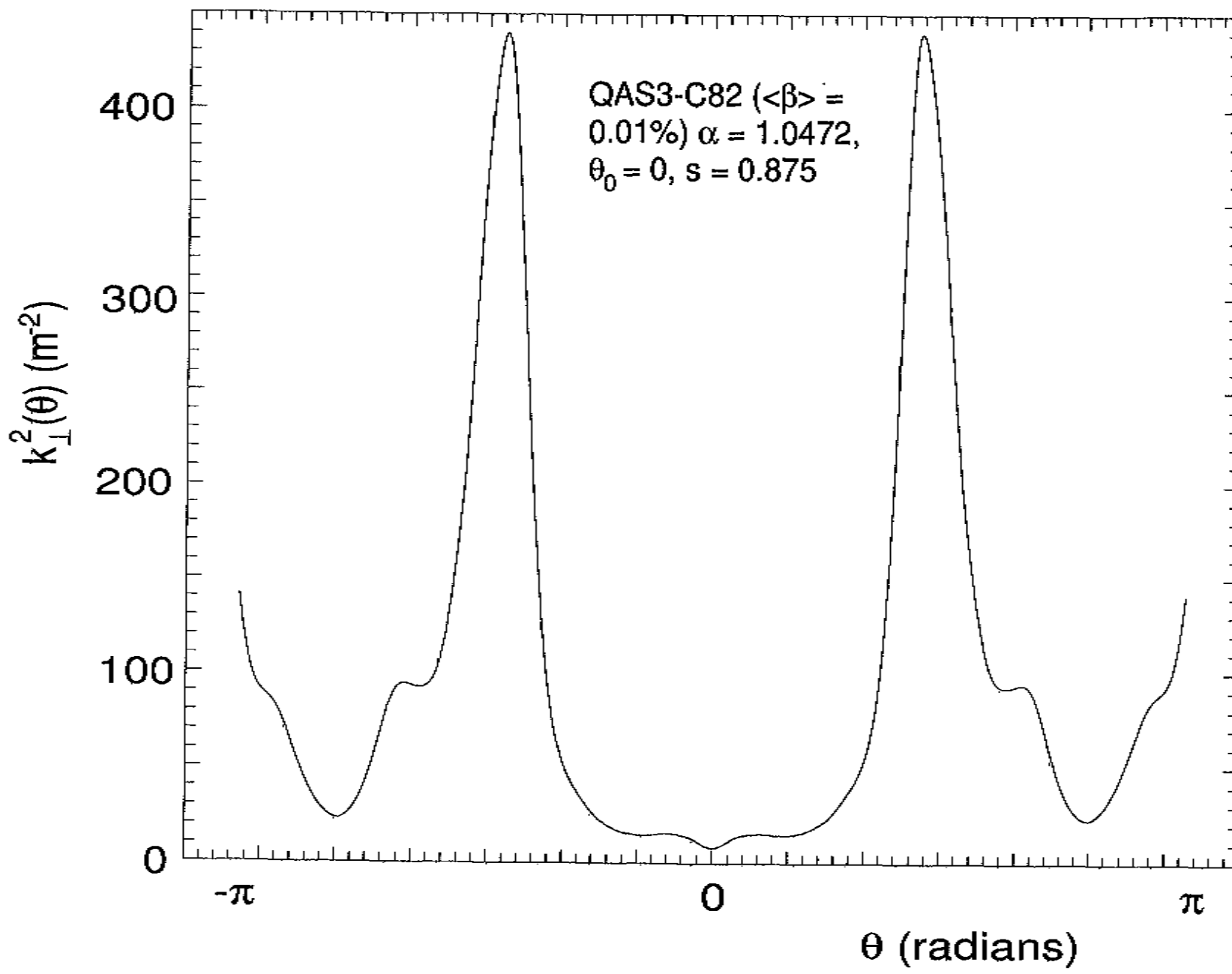


Fig. 4

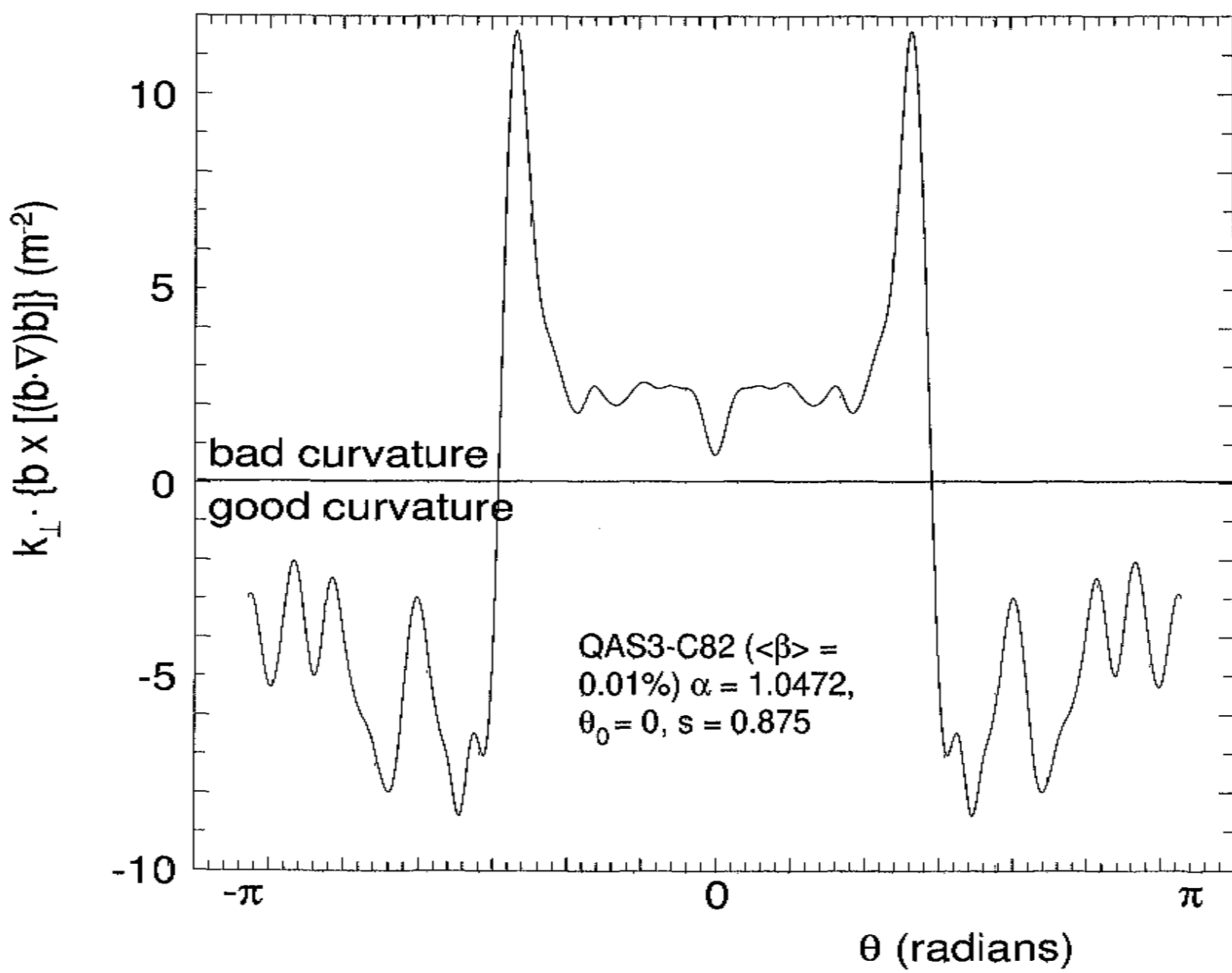
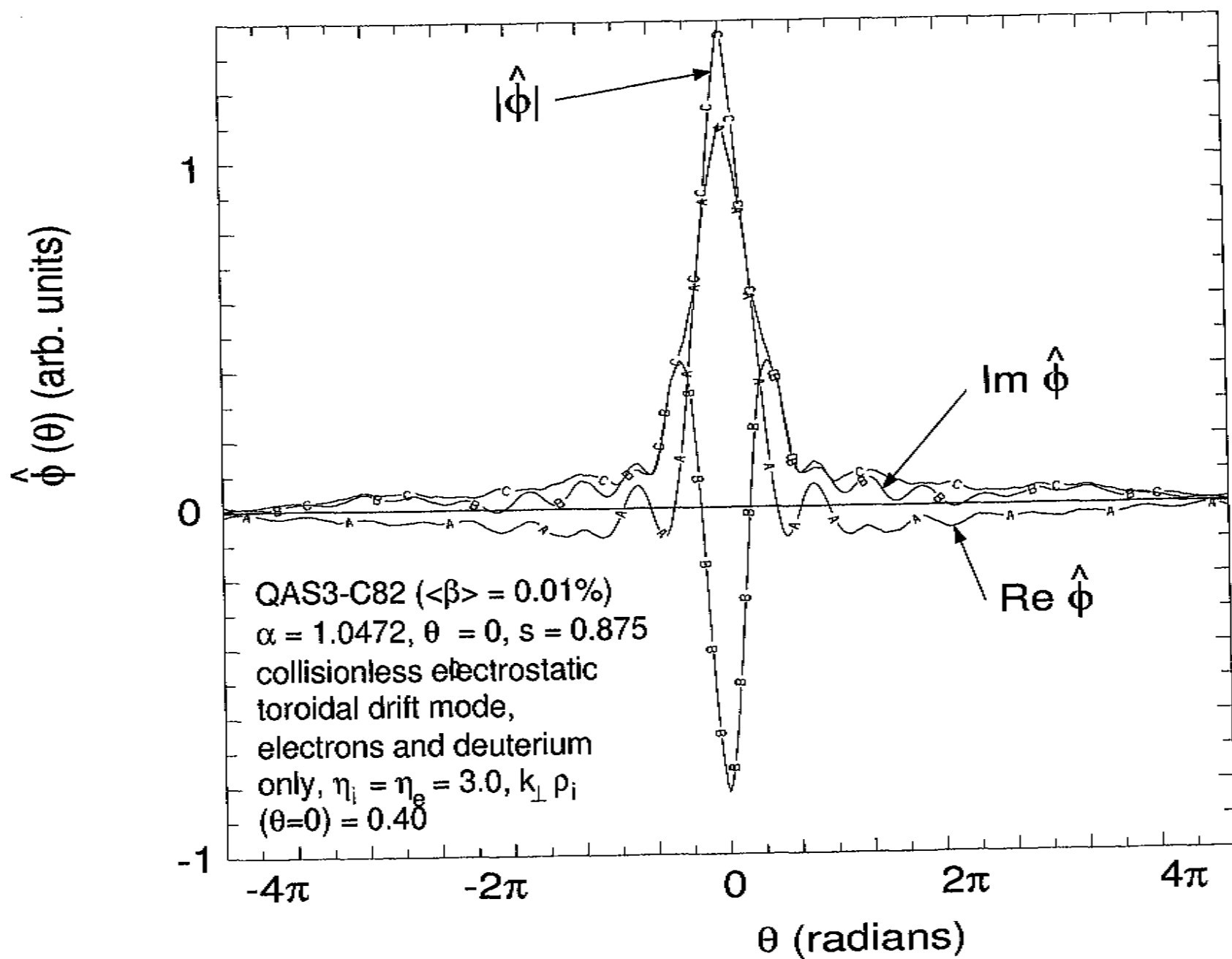


Fig. 5

- Corresponding eigenfunction for perturbed electrostatic potential  $\tilde{\phi}$  versus non-periodic ballooning coordinate  $\theta$  shown in Fig. 6 for  $\eta_i = \eta_e = 3.0$  and  $k_{\perp} \rho_i(\theta = 0) = 0.40$ , without collisions. Mainly localized within toroidal magnetic field well around  $\theta = 0$ , and overlaps outlying helical wells only very weakly
- Results shown for linear growth rate  $\gamma$  versus  $\eta_i = \eta_e$  for collisionless (and collisional) electrostatic toroidal drift modes (trapped-electron and ITG modes) in Fig. 7, for  $k_{\perp} \rho_i(\theta = 0) = 0.40$  or  $n = 25$  for ITG root and  $k_{\perp} \rho_i(\theta = 0) = 0.43$  or  $n = 27$  for TEM root, with only electrons and background deuterium ions. Corresponding results for real frequency  $\omega_r$  shown in Fig. 8. In these figures, total pressure gradient held fixed as  $\eta_i = \eta_e$  varies, so that density gradient decreases as electron and ion temperature gradients increase, and vice-versa.



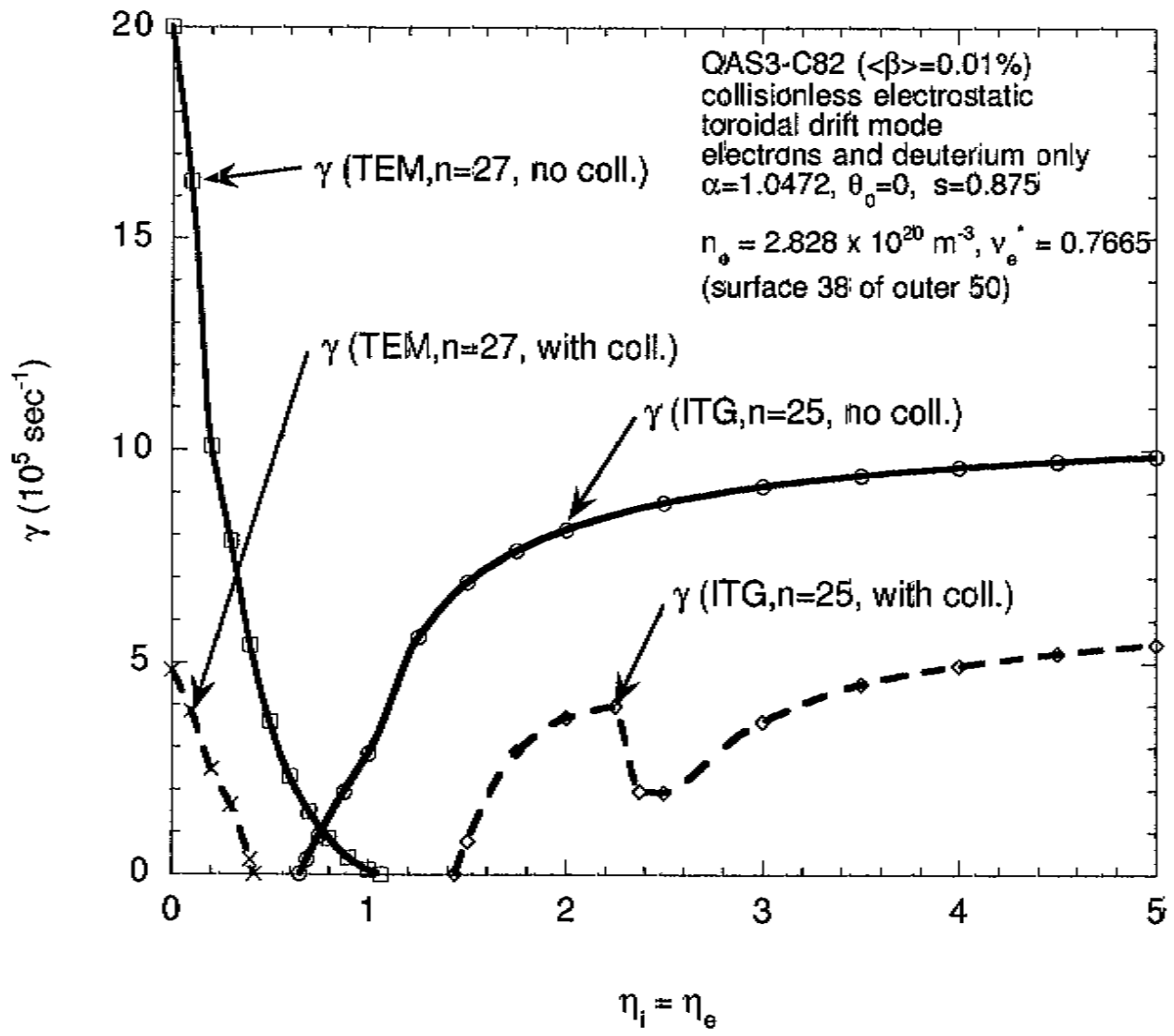


Fig. 7

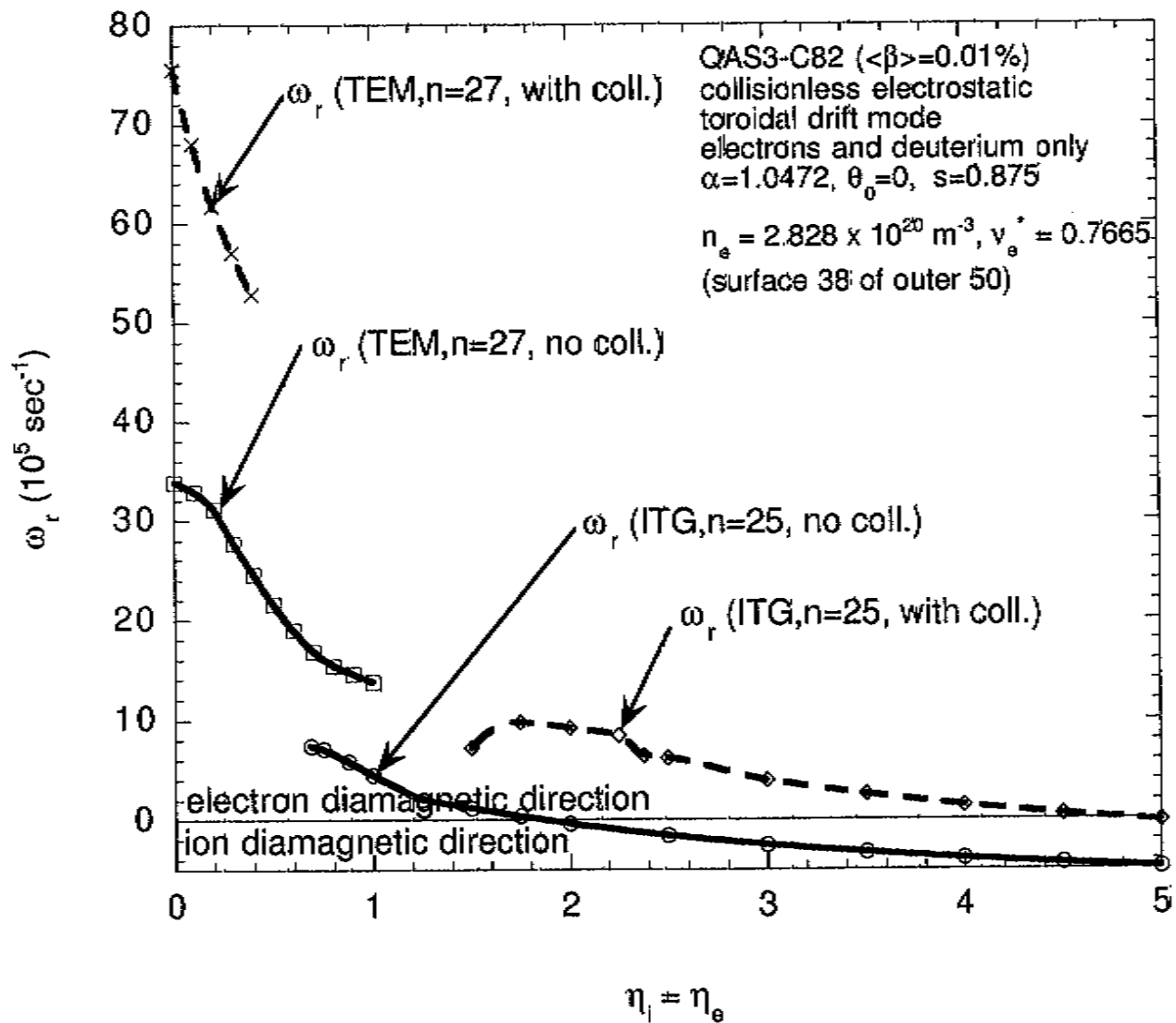


Fig. 8

- Two separate roots found, corresponding to collisionless or collisional trapped electron mode (TEM) and to ion temperature gradient (ITG) mode (including trapped-particle effects). For this case, they do not hybridize, unlike many typical tokamak cases.
- Variation of  $\gamma$  and  $\omega_r$  with  $k_{\perp}\rho_i(\theta = 0)$  or  $n$  is shown in Fig. 9 for collisionless ITG mode with  $\eta_i = \eta_e = 3.0$  and for collisionless TEM mode with  $\eta_i = \eta_e = 0.0$ . Eigenfrequency has  $k_{\perp}\rho_i$  dependence that is familiar for tokamaks, with growth rate peaks for  $k_{\perp}\rho_i(\theta = 0) \simeq 0.4$  to 0.5, and transition of real frequency from electron to ion diamagnetic direction for ITG root. TEM root stays in electron diamagnetic direction
- Effect of varying ballooning parameter  $\theta_0$  ( $= \theta_k$ ) is shown in Fig. 10.  $\theta_0 = 0$  is most unstable for this case. Effect

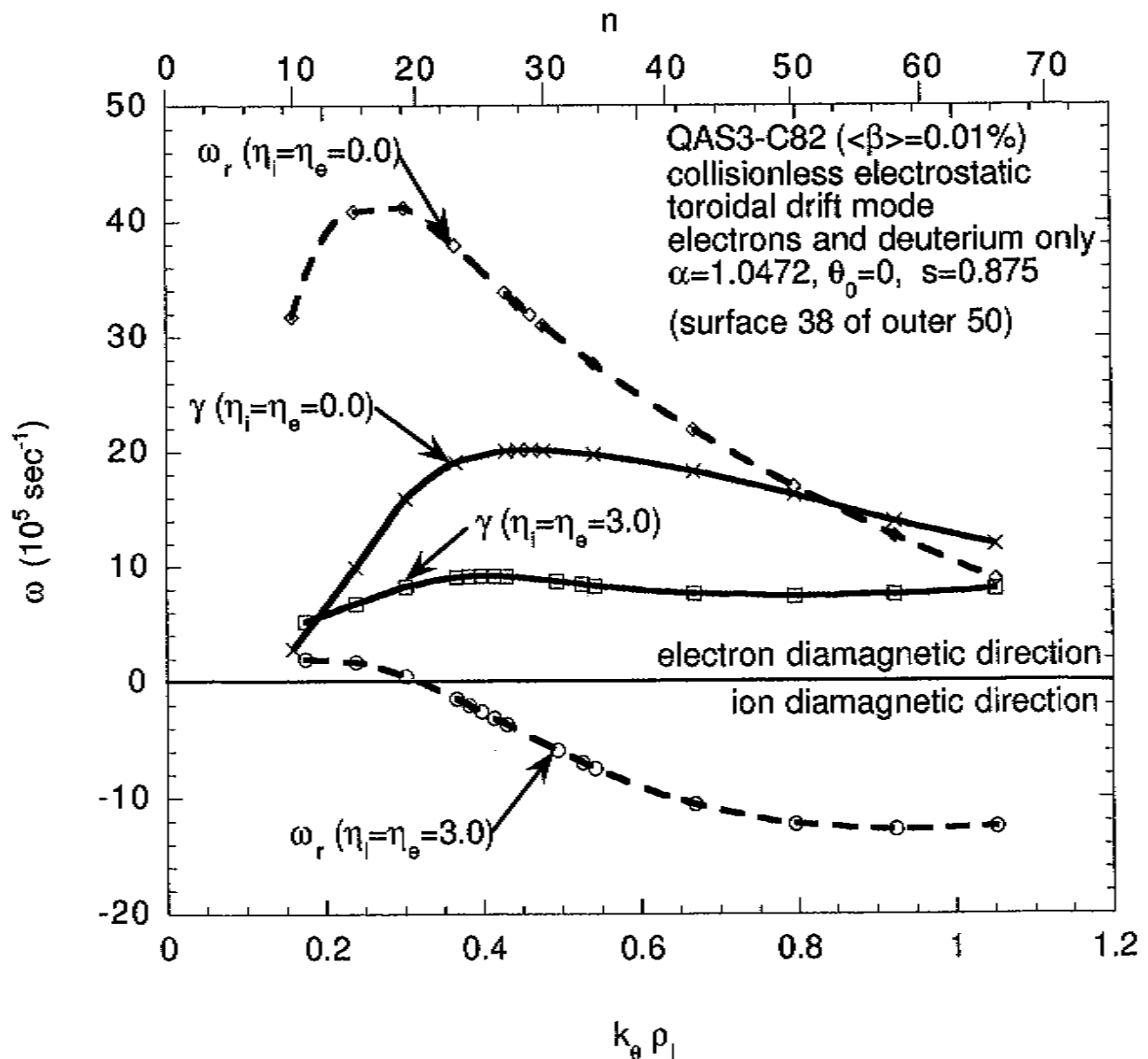


Fig. 1

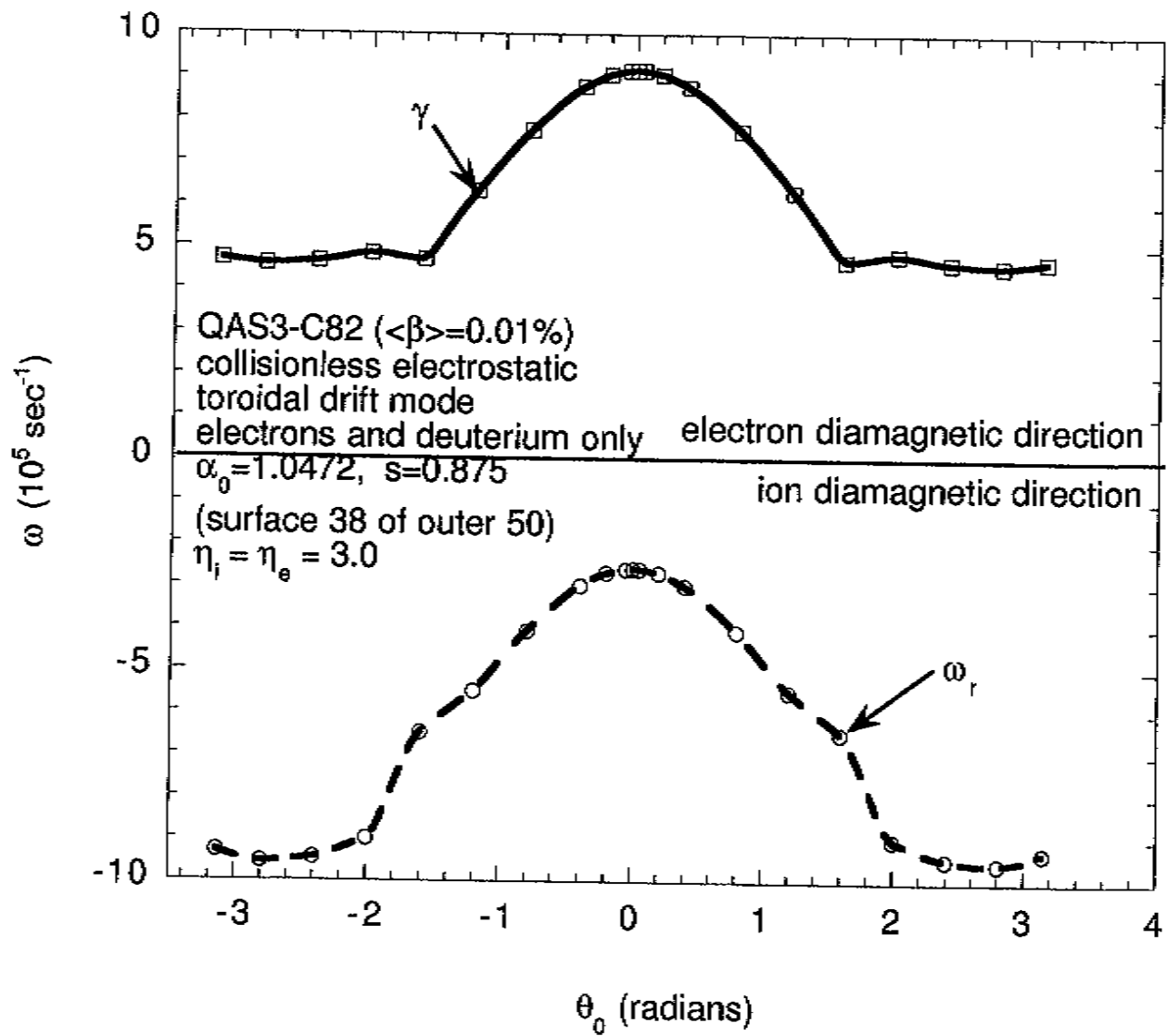


Fig. 10

of varying field line label  $\alpha \equiv \zeta - q\theta$  is shown in Fig. 11.  
 $\alpha = \pi/3 = 1.0472$  is most unstable for this case

- Effect of varying  $T_e/T_i$  are shown in Fig. 12. Little effect when varying  $T_i$  at fixed  $T_e$  and fixed  $k_\theta \rho_i$ , but increasing  $T_e$  destabilizing at fixed  $T_i$
- Radial scan of  $\gamma$  and  $\omega_r$  for ITG root shown in Fig. 13. Broad region of instability (and presumed anomalous transport)

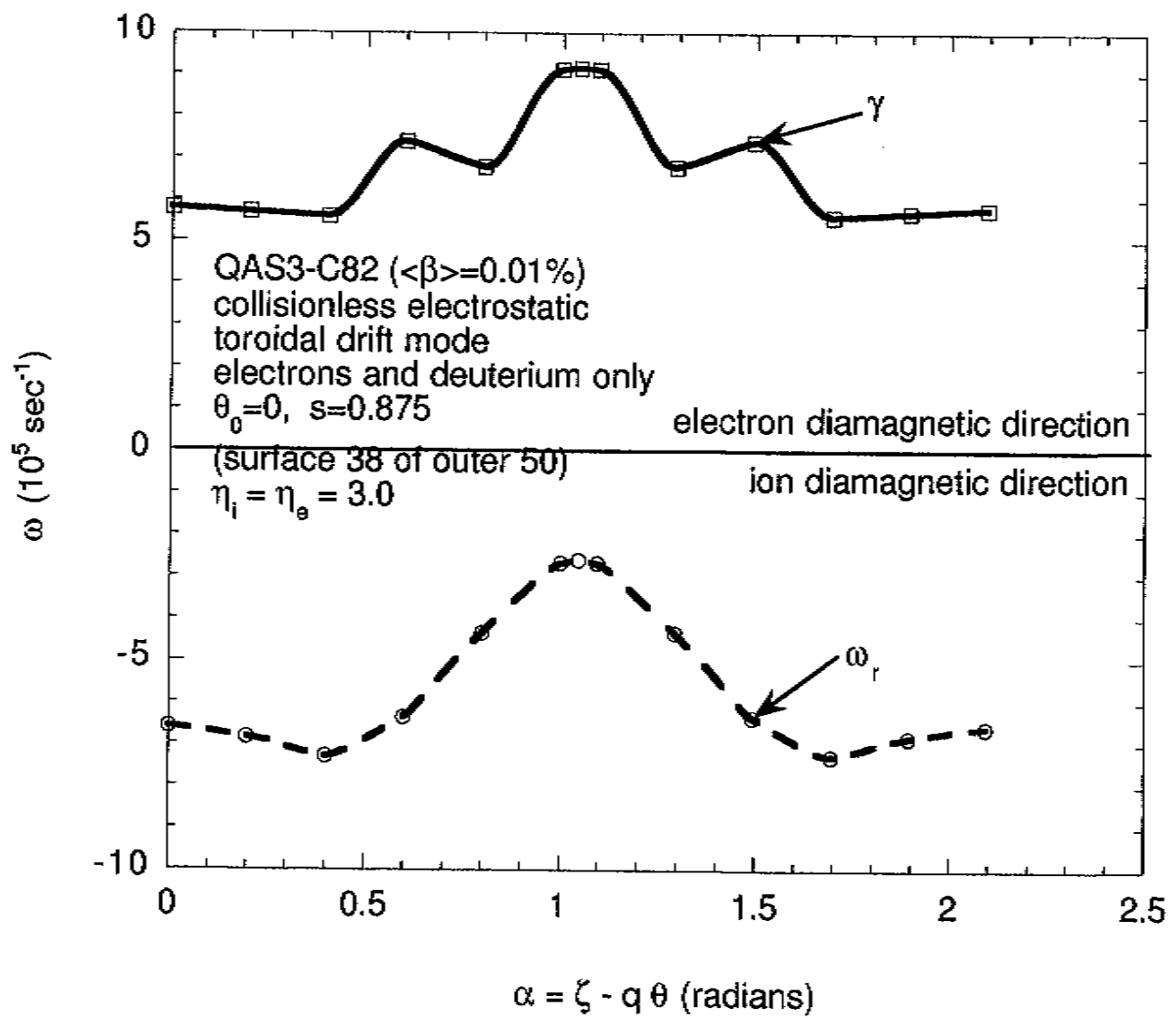


Fig. 11

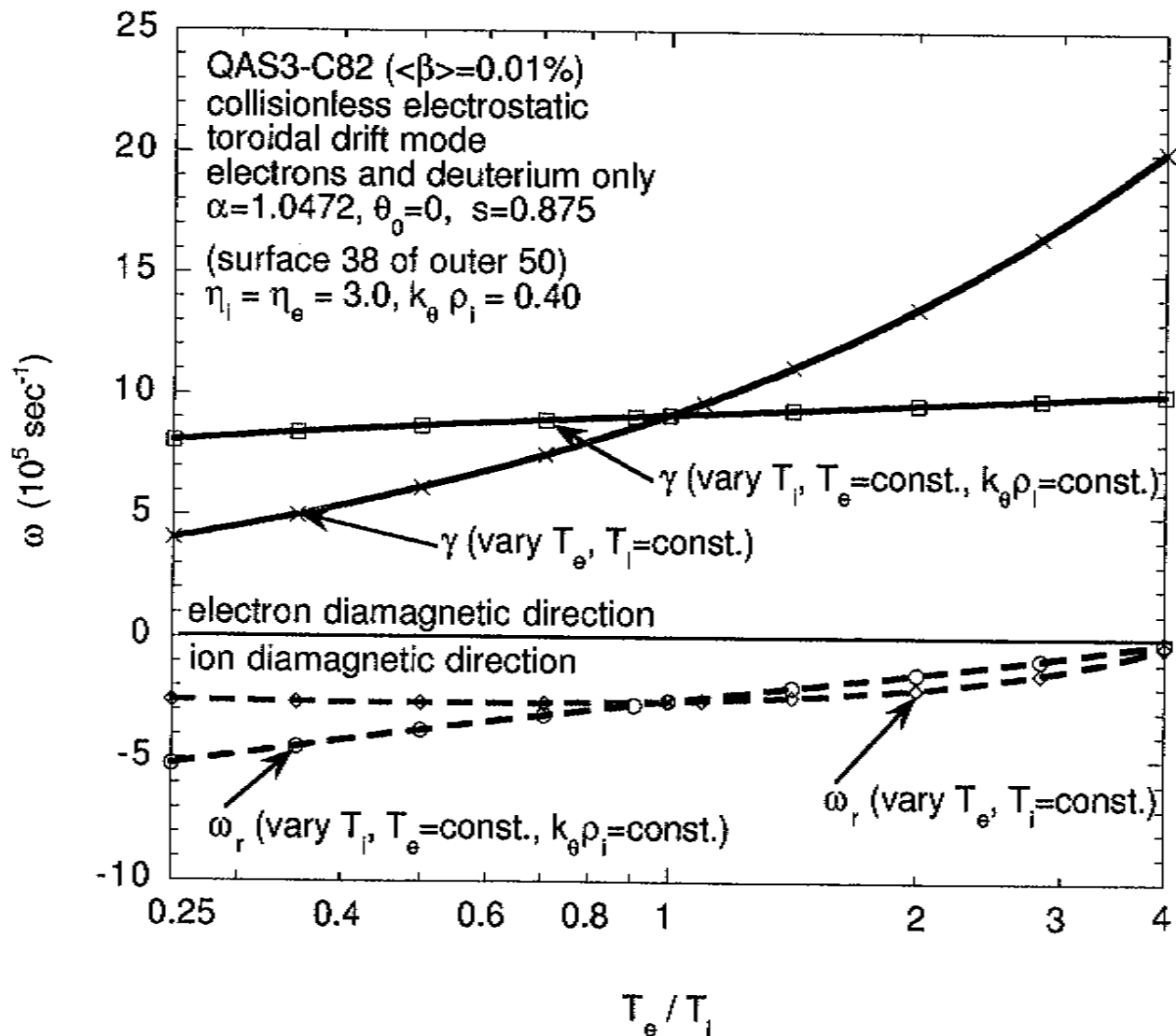


Fig. 12

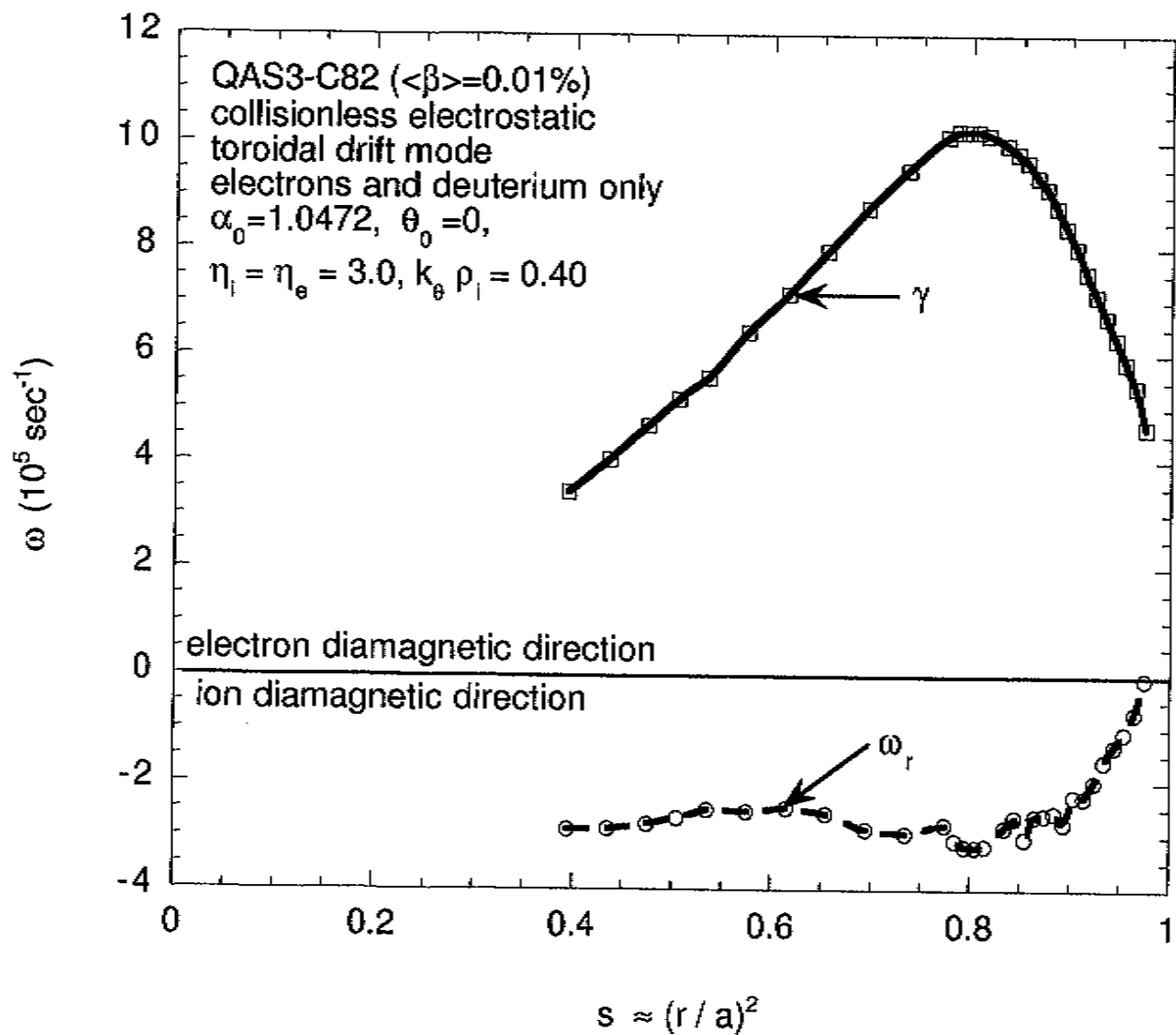


Fig. 13

# COLLISIONAL EFFECTS

---

- Axisymmetric FULL code uses model Krook collision operator to approximate physical process of two-step de-trapping and retrapping
- Gives effective collision frequency which diverges in pitch angle at trapped-passing boundary
- Good agreement with results from equivalent calculation using Lorentz operator
- In nonaxisymmetric version, where there are multiple classes of trapped particles, generalize to include transitions between adjacent trapped-particle classes also

- FULL code finds all local maxima of  $|B|(\theta)$  (minima of  $h(\theta) \equiv B_0/B(\theta)$ ), and  $\nu_{efj}$  is constructed to diverge (in pitch angle) at these maxima, modeling behavior of Lorentz collision operator, as illustrated in Fig. 14
- Behavior of  $\gamma$  and  $\omega_r$  with collision frequency (density) for ITG and TEM roots is shown in Figs. 15 and 16
- Variation of  $\gamma$  and  $\omega_r$  with  $\eta_i = \eta_e$  including collisions is shown in Figs. 7 and 8

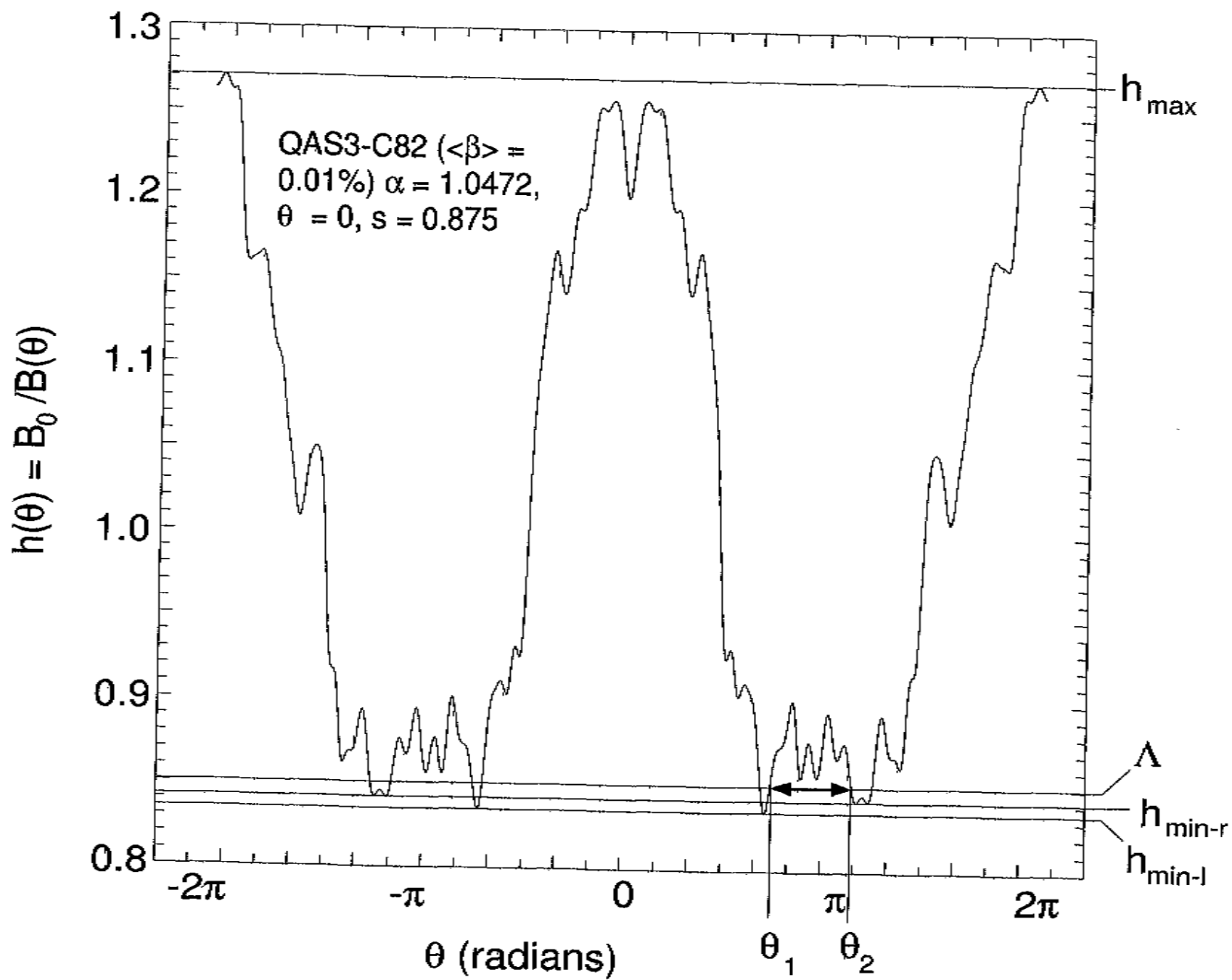


Fig. 14'

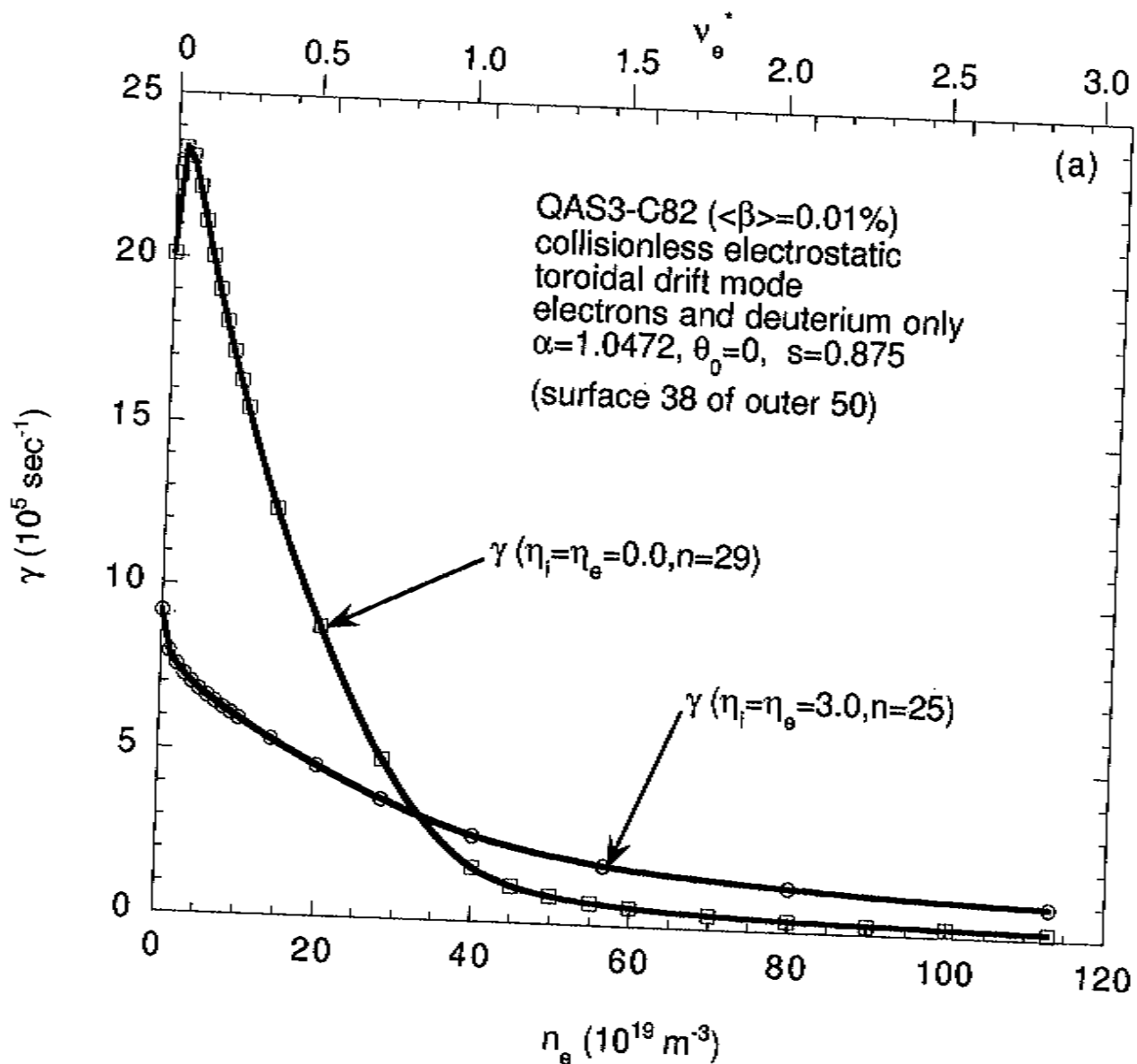


Fig. 15

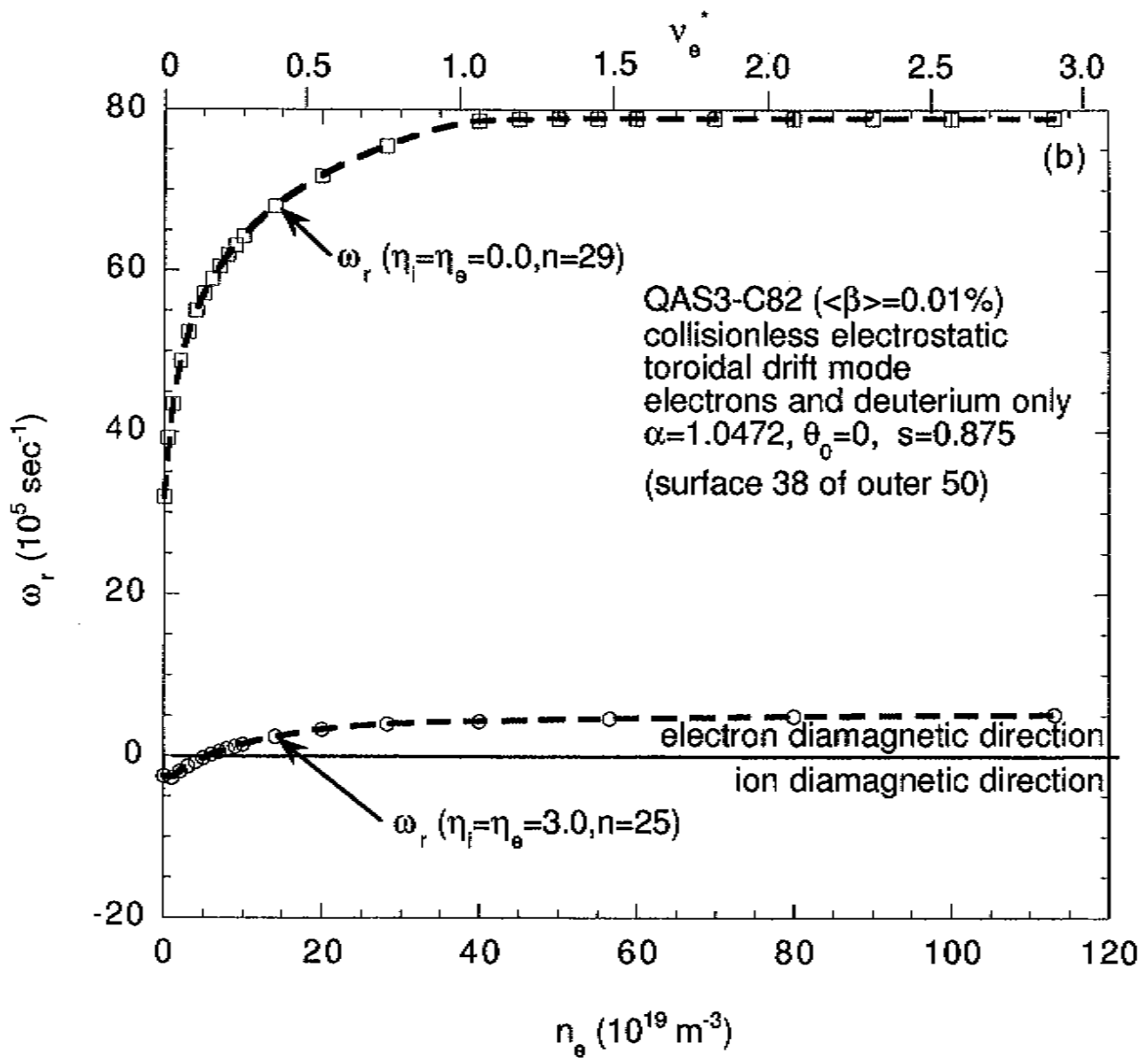


Fig. 16

# CONCLUSIONS AND FUTURE PLANS

---

- Have converted existing tokamak (axisymmetric) linear microinstability code FULL to stellarator (nonaxisymmetric) code, with same kinetic effects included, for electrostatic version
- Data for nonaxisymmetric FULL code obtained using 3D VMEC MHD equilibrium code, and TERPSICHORE and VVBAL MHD stability codes
- Good agreement obtained between tokamak and stellarator versions of FULL code using matched 2D (JSOLVER) and 3D (VMEC) MHD equilibria

- Results obtained for collisionless and collisional electrostatic toroidal drift mode (trapped-electron-ITG mode) for stellarator case. Separate unstable TEM and ITG roots have properties in common with tokamak results
- Future extensions will include fully electromagnetic version, rotation model, etc.
- Will apply nonaxisymmetric FULL code to future iterations of NCSX stellarator design, to LHD, and to other stellarators